GH3-mediated auxin inactivation attenuates multiple stages of lateral root development

Qing Wang[1,2], Hugues De Gernier[1,2], Xingliang Duan[5], Yuanming Xie[5], Danny Geelen[3], Ken-Ishiro Hayashi[6], Wei Xuan[5], Markus Geisler[4], Kirsten ten Tusscher[7], Tom Beeckman[1,2*], Steffen Vanneste[1,2,3*]

[1] Department of Plant Biotechnology and Bioinformatics, Ghent University, Ghent 9052, Belgium.

[2] Center for Plant Systems Biology, VIB-UGent, Ghent 9052, Belgium.

[3] Department of Plants and Crops, Faculty of Bioscience Engineering, Ghent University, Ghent 9000, Belgium.

[4] Department of Biology, University of Fribourg, CH-1700 Fribourg, Switzerland.

[5] MOA Key Laboratory of Plant Nutrition and Fertilization in Lower-Middle Reaches of the Yangtze River and State Key Laboratory of Crop Genetics and Germplasm Enhancement, Nanjing Agricultural University, Nanjing 210095, China.

[6] Department of Biochemistry, Okayama University of Science, Okayama 700-0005, Japan.

[7] Computational Developmental Biology Group, Faculty of Science, Utrecht University, Utrecht 3584 CH, The Netherlands

*Correspondence: Tom.Beeckman@psb.vib-ugent.be ; Steffen.Vanneste@UGent.be

ORCID:

Qing Wang 0000-0002-5903-7938 ; Hugues De Gernier 0000-0002-7644-3233; Xingliang Duan 0000-0002-2218-9014 ;Yuanming Xie 0009-0007-5798-7407; Danny Geelen 0000-0001-8105-3937 ;Ken-Ishiro Hayashi 0000-0002-9812-2801 ;Wei Xuan 0000-0002-4859-2637 ;Markus Geisler 0000-0002-6641-5810 ;Kirsten den Tusscher 0000-0002-1945-7858 ; Tom Beeckman 0000-0001-8656-2060 ; Steffen Vanneste 0000-0002-9948-9672

Summary

- Lateral root (LR) positioning and development rely on the dynamic interplay between auxin production, transport but also inactivation. Nonetheless, how the latter affects LR organogenesis remains largely uninvestigated.
- Here, we systematically analyze the impact of the major auxin inactivation pathway defined by GRETCHEN HAGEN3-type (GH3) auxin conjugating enzymes and DIOXYGENASE FOR AUXIN OXIDATION1 (DAO1) in all stages of LR development using reporters, genetics and inhibitors.
- Our data demonstrate that the *gh3.1/2/3/4/5/6* hextuple (*gh3hex*) mutants display a higher LR density due to an increased LR initiation and faster LR developmental progression, acting epistatically over *dao1-1*. Grafting and local inhibitor applications reveal that root and shoot GH3 activities control LR formation. The faster LR development in *gh3hex* is associated with GH3 expression domains in and around developing LRs. The increase in LR initiation is associated with accelerated auxin response oscillations coinciding with increases in apical meristem size and lateral root cap cell death rates.
- Our research reveals how GH3-mediated auxin inactivation attenuates LR development. Local GH3 expression in LR primordia attenuates development and emergence, whereas GH3 effects on pre-initiation stages is indirect, by modulating meristem activities that in turn coordinate root growth with LR spacing.

Key words: auxin, auxin conjugation, DAO1, GH3, lateral root, oscillation, root

INTRODUCTION

The plant hormone auxin is a major activating signal for lateral root (LR) development. Its local accumulation in xylem-pole pericycle (XPP) cells is the rate-limiting event that controls onset of LR formation (De Smet *et al.*, 2007; Dubrovsky *et al.*, 2008; De Rybel *et al.*, 2010). The nuclear auxin signaling reporter *DR5::Luciferase* (*DR5::LUC*), together with the expression of many other genes, was found to oscillate in a region proximal to the meristem, designated as the oscillation zone. These oscillations have been demonstrated to position root pre-branch sites (PBS) along the primary from which future LRs may arise, thereby controlling LR spacing (Moreno-Risueno *et al.*, 2010; Xuan *et al.*, 2020). While not every PBS develops into a LR, each LR derives from a PBS, suggesting that the efficiency with which priming is translated to PBS is a further major factor determining root branching (Van Norman *et al.*, 2013). Interestingly, priming and subsequent PBS formation is highly dependent on canonical auxin signaling in the stele (Xuan *et al.*, 2015), suggesting that it is the oscillatory auxin signal that determines the root branching pattern. This notion is supported by the observation that the amplitude of the oscillatory *DR5::LUC* needs to be sufficiently high for it to translate into a stable PBS (Xuan *et al.*, 2015). This implies that weak auxin oscillations are dissipated and forgotten, while stronger ones are memorized for subsequent formation of a PBS with intense auxin signaling. Modeling work suggests that the amplitude of auxin oscillations depends on overall root tip auxin availability (van den Berg *et al.*, 2021), and that sufficient oscillation amplitude as well as local auxin biosynthesis contribute to successful PBS formation (Laskowski & Ten Tusscher, 2017; Santos Teixeira *et al.*, 2022).

Additionally, auxin availability is known to promote LR development, also beyond the PBS stage. A first morphological hallmark of subsequent LR development is the coordinated asymmetric cell division of XPP cells, followed by periclinal cell division to start building the LR primordium (LRP). Within the incipient LRP, auxin signaling levels set the pace for its development (Guseman *et al.*, 2015). During its development, auxin gradients emerge to organize the cell identities and establish a functional new meristem (Benkova *et al.*, 2003). At the same time, auxin signaling is activated in the tissues that overlay a LRP, to facilitate LRP emergence (Stoeckle *et al.*, 2018). These examples demonstrate the importance of auxin homeostasis in all stages of LR development.

Auxin biosynthesis, transport, reversible conjugation and irreversible catabolism jointly make up a set of complex mechanisms that jointly control the auxin distributions patterns that regulate plant growth and development.

Glycosylation, amino acid conjugation and methylation are the main pathways for inactivating indole-3-acetic acid (IAA) (Casanova-Saez *et al.*, 2021). Each of these reactions is reversible, and thus allows for flexible release of auxin without the need for *de novo* auxin biosynthesis. A subgroup of Gretchen Hagen3-type (GH3) acyl acid amido synthases (group II) can conjugate IAA to amino acids (Staswick *et al.*, 2005). Of the eight Group II GH3 proteins in Arabidopsis (*Arabidopsis thaliana*) acting as auxin-inactivating enzymes, GH3.1 to GH3.6 conjugate IAA preferentially to aspartate (Asp) while GH3.9 and GH3.17 have a preference for conjugating IAA to glutamate (Glu) to attenuate the auxin response (Staswick *et al.*, 2005; Ludwig-Muller, 2011; Sugawara *et al.*, 2015). Consistently with this enzymatic preference, *gh3.1/2/3/4/5/6* mutants lost the ability to form IAA-Asp, but not IAA-Glu (Porco *et al.*, 2016), while *gh3.17* mutants display a strong reduction in IAA-Glu, but not in IAA-Asp (Zheng *et al.*, 2016). Octuple *gh3.1/2/3/4/5/6/9/17* mutants completely lost the ability to form IAA-Asp and had strongly reduced IAA-Glu levels (Casanova-Saez *et al.*, 2022; Guo *et al.*, 2022).

Release of IAA from IAA-amino acid conjugates is catalyzed by endoplasmic reticulum-localized ILR/ILLs (IAA-Leu-Resistant1/ILR-likes) (Sanchez Carranza *et al.*, 2016). Recently, it was found that DIOXYGENASE FOR AUXIN OXIDATION1 (DAO1) is required for the irreversible oxidative degradation of IAA, as indicated by the severe reduction or even complete loss of 2-oxindole-3-acetic acid (oxIAA) in *dao1* loss-of-function alleles (Mellor *et al.*, 2016; Porco *et al.*, 2016; Takehara *et al.*, 2020). Instead of the originally proposed direct oxidation of IAA to 2-oxindole-3-acetic acid (oxIAA), it seems that DAO1 preferentially oxidizes IAA-amino acids (Hayashi *et al.*, 2021; Müller *et al.*, 2021). This explains why IAA-Asp and IAA-Glu levels are increased while oxIAA-Asp and oxIAA-Glu are absent in *dao1-1* (Hayashi *et al.*, 2021; Müller *et al.*, 2021). The reduction of oxIAA in *gh3.1/2/3/4/5/6/17* and *gh3.1/2/3/4/5/6/9/17* and precursor feeding experiments (Hayashi *et al.*, 2021; Casanova-Saez *et al.*, 2022), further support a model in which GH3-mediated IAA-amino acid conjugation is an important entry-point for irreversible auxin degradation, acting upstream of DAO1 (Hayashi *et al.*, 2021).

Since their identification, GH3 proteins have been proposed as part of an important auxin attenuation mechanism, based on their auxin conjugating enzymatic activity and gain-of-function phenotypes (Takase *et al.*, 2004; Staswick *et al.*, 2005; Nakazawa *et al.*, 2008). Single mutant phenotypes in *Arabidopsis* have only been described for *GH3.17*, in the context of shade avoidance responses in the hypocotyl (Zheng *et al.*, 2016) and meristem size through cytokinin-regulated expression in the lateral root cap (LRC) (Di Mambro *et al.*, 2019). Single mutants in *gh3.5* and *gh3.6* display longer meristems, similarly to *gh3.17* (Pierdonati et al., 2019), and *gh3.3*, *gh3.5* and *gh3.6* develop more adventitious roots in etiolated seedlings (Gutierrez *et al.*, 2012). None of the single mutants in group II *gh3* were found to have strong root growth or LR phenotypes (Gutierrez *et al.*, 2012; Xuan *et al.*, 2015; Guo *et al.*, 2022). Recently, LR development of *gh3.15/gh3.9* double mutant in tomato was reported to be less sensitive to inhibition of auxin transport (Ai *et al.*, 2023). In Arabidopsis, hextuple , septuple and octuple group II *gh3* mutants have progressively more prominent root phenotypes (Mellor *et al.*, 2016; Porco *et al.*, 2016; Zhang *et al.*, 2016; Casanova-Saez *et al.*, 2021; Hayashi *et al.*, 2021; Guo *et al.*, 2022), highlighting their importance in root development. The availability of higher order mutants and selective inhibitors of group II GH3s, such as kakeimide (KKI) (Fukui *et al.*, 2022), allows to overcome group II GH3 functional redundancy and explore their role in plant development.

Here, we use these tools to determine how GH3 and DAO1 activities contribute to the dynamic changes in active auxin pools in the plant that drive LR development. Genetic interaction revealed epistatic interactions of *gh3hex* over *dao1-1* in various stages of LR development. Using a systematic approach we could demonstrate that localized GH3 activities control not only the speed of LR development and emergence, but also the initiation of new LRs via increasing the frequency of oscillation amplitudes related to meristem size changes without dramatically increasing root growth rate. Grafting revealed that GH3 controlled pools of auxin in the shoot contribute to LR development. Jointly, these data reveal an intricate connection between GH3 activities and control of LR development at multiple levels.

MATERIALS AND METHODS

Plant materials and growth conditions

Arabidopsis seeds were surface-sterilized for 15 min in 10% bleach, washed four times with sterile water, and plated on 0.5xMS medium with 0.8% agar. Plants were stratified at 4℃ for 2 or 3 days in darkness and then transferred to a growth chamber at 21℃ under continuous illumination (light intensity 120 µmol m^{-2} s^{-1}). *Arabidopsis thaliana* ecotype Col-0 was used as WT control. The following lines/seeds/constructs were used in this study: *dao1-1* (SALK_093162) (Porco *et al.*, 2016), *gh3.1-6* (Porco *et al.*, 2016), *aux1-21* (CS9584) (Swarup *et al.*, 2004), *DR5rev:3×VENUS-N7* (Heisler *et al.*, 2005), *DR5::LUC* (Moreno-Risueno *et al.*, 2010), *GH3.1pro::NLS-GFP/GUS*, *GH3.2pro::NLS-GFP/GUS*, *GH3.3pro::NLS-GFP/GUS*, *GH3.4pro::NLS-GFP/GUS*, *GH3.5pro::NLS-GFP/GUS*, *GH3.6pro::NLS-GFP/GUS* lines were generated through Agrobacterium-mediated floral dip transformation (Clough & Bent, 1998).

Genotyping

Crosses were made among *dao1-1*, *gh3hex*, *aux1-21*, *DR5::LUC* and *DR5rev:3×VENUS-N7* reporters. The genotypes were determined by PCR and sequencing (Swarup *et al.*, 2004; Porco *et al.*, 2016). DNA was extracted from a single leaf of young seedlings using CTAB DNA extraction as described previously (Clarke, 2009).

GUS staining and microscopy

The ß-glucuronidase (GUS) assays were performed as previously described (Beeckman & Engler, 1994). For microscopic analysis, samples were cleared by mounting in lactic acid (Acros Organics, Geel, Belgium) or as described previously (Malamy & Benfey, 1997). In brief: Incubate seedlings in acetone 90% overnight at 4℃ or until completely white. Transfer seedlings to a new plate containing phosphate buffer (0.5M, pH 7.0) for 30min at 37℃. Replace phosphate buffer by Solution I (2ml HCL, 20% Methanol in 100ml of water) and incubate 45min at 60℃. Replace by Solution II (7% NaOH and 60% EtOH) and incubate 15min at room temperature. Wash with 40%, 20%, 10% of EtOH 5 min, respectively. Mount seeding with 50% glycerol on slides for microscopic analysis . All samples were analyzed using a BX53 Olympus microscope.

Phenotyping and statistics

For analyzing stages of LRP development plant material was cleared following the protocol as described (Malamy & Benfey, 1997). LRP density was calculated as the ratio of the total number of LRP over the sum of root length. The counting of LRP was performed in the direction from root tip towards the root base. Root lengths were analyzed using Image J software (http://rsb.info.nih.gov/ij). For macroscopic root phenotyping, the number of emerged LRs was determined using a stereomicroscope. Statistical analysis was performed by two-tailed t-test, One-way ANOVA Graph Pad and two-way ANOVA Graph Pad.

Confocal Microscopy

For auxin distribution of *DR5rev:3×VENUS-N7* Zeiss LSM 710 confocal microscope with a ×20 objective with GFP settings (excitation 488 nm, emission 507 nm) was used to identify and analyze *DR5rev:3×VENUS-N7* positive signals in the root tip. Cell walls were stained with propidium iodide (10 µg/mL; Sigma).

For meristem size assays, roots of PI-stained seedlings were analyzed by confocal microscopy (Zeiss LSM 710) and the number of non-elongated cortex cells in median plane of the meristem was counted.

Cloning

To construct *GH3pro::NLS-GFP/GUS*, a GH3s promoter region (±2.2 kb upstream of translational start) was amplified with using GH3.1_pr_F GGGGACAACTTTGTATAGAAAAGTGGTAATGAGAACCTAACTCATAATC, GH3.1_pr_R GGGGACTGCTTTTTTGTACAAACTTGTATGTTTTAGCTATTTG, GH3.2_pr_F GGGGACAACTTTGTATAGAAAAGTGGTACCGTGCGATTAGCC TCTTCCT, GH3.2_pr_R GGGGACTGCTTTTTTGTACAAACTTGTATTTGTTTTTT TTTCTAAAAGAAAAAGTG, GH3.3_pr_F GGGGACAACTTTGTATAGAAAAGTG GTATCTTACCAAGATACCACCGTAT, GH3.3_pr_R GGGGACT GCTTTTTTGTACAAA CTTGTGATTAAAATGGTATTTGTAAGTG, GH3.4_pr_F GGGGACAACTTTGTATAG AAAAGTGGTATAGCGTTCCACACAGACGACGCCA GH3.4_pr_R GGGGACTG CTTTTTTGTACAAACTTGTGATTTATCGAATGTTTTTGTG GH3.5_pr_F GGGGACA ACTTTGTATAGAAAAGTGGTAAGATGTGCGACAGTTGAAACTACTG GH3.5_pr_R GGGGACTGCTTTTTTGTACAAACTTGTGGTTTAAGAGAAAGAGAGAAGTC; GH3.6_pr_F GGGGACAACTTTGTATAGAAAAGTGGTACCATTAACAGCAGACGTT ATCT; GH3.6_pr_R

GGGGACTGCTTTTTTGTACAAACTTGTCGTTTAGGTTTTG TGTT and cloned into pDONR^{TM}P4-P1R. GH3pro in pDONR^{TM}P4-P1R was sub-cloned into pEX-K7SNFm14GW to construct *GH3pro::NLS-GFP/GUS* with the Multisite Gateway two-fragment vector construction kit (Invitrogen).

Agrobacterium and Arabidopsis transformation

Agrobacterium tumefaciens strain GV3101 was transformed with the relevant binary plasmids via the freeze-thaw procedure (Weigel & Glazebrook, 2006). For each construct, an individual, PCR-confirmed, Agrobacterium colony was used to start a culture for floral dip (Clough & Bent, 1998). Transformants were selected and single locus lines were selected based on their segregation ratios of the T2 generation.

Luciferase activity imaging and expression analysis

The luminescence emitted by the *DR5::LUC* plants was detected using charge-coupled device (CCD) cameras integrated either in a Lumazone recording unit (Xuan *et al.*, 2018) or a Nightshade LB985 (BERTHOLD TECHNOLOGIES) imaging environment. The Nightshade LB985 system was used to monitor the changes of *DR5::LUC* expression overtime, in newly-grown root regions above the apex. To do so, the luminescence was captured every 15 minutes, with an exposure time of 10 minutes), during ~22 hours. Before imaging, the 3DAG seedlings were transferred to new plates with or without chemical, and then were sprayed with 1 mM D-luciferin solution (Duchefa Biochemie). After imaging, the picture series were saved as 8-bit images in TIFF format for further analysis. To quantify the amplitude and frequency of *DR5::LUC* expression peaks in the oscillation zone, we followed the kymograph analysis method described in (Xuan *et al.*, 2018; van den Berg *et al.*, 2021). The analysis was performed in ImageJ (Schneider *et al.*, 2012). In brief, the *DR5::LUC* expression in the oscillation zone was quantified as the gray value of the corresponding pixel region. To visualize the changes of expression in the oscillation zone, we first traced a segmented line, fitting the primary root at the last time point, then generated a kymograph (http://www.embl.de/eamnet/html/body_kymograph.html). This allows to display in a two-dimension graph the temporal changes of *DR5::LUC* expression at each position along the primary root. In a kymograph, the oscillatory changes of *DR5::LUC* expression are typically

distributed along a diagonal line (Xuan *et al.*, 2018). Second, a plot profile was produced along that line to reveal the periodic expression peaks. The oscillation amplitude of each peak was calculated as the difference between the maximum gray value and the minimum preceding it. The periodicity of the *DR5::LUC* oscillations was calculated by recording the time interval between consecutive expression peaks.

The Lumazone system was used to assess the pattern of *DR5::LUC* expression along the whole primary root in order to count the PBS number. To achieve this, 6-day-old seedlings, WT or mutant individuals harboring the *DR5::LUC* construct were sprayed with D-luciferin and the emitted light captured with a 20 min exposure time. Static *DR5::LUC* expression sites that were visible along the primary root outside the oscillation zone were counted as PBS.

Polar auxin transport (PAT) measurements

Shoot-to-root (acropetal) PAT measurements allowing to simultaneously quantify ^{3}H-IAA and ^{14}C-BA transport were essentially performed as described (Lewis & Muday, 2009). 5% agarose beads containing each 100 nM ^{3}H-IAA (specific activity 20 Ci mmol^{-1}; American Radiolabeled Chemicals, Inc., St. Louis, MO) and ^{14}C-BA (specific activity of 50 Ci mmol^{-1}; American Radiolabeled Chemicals, Inc., St. Louis, MO), respectively, were placed in close proximity above the shoot tip of seedlings (see Fig. **2f** for details) aligned on vertically oriented ½ MS plates supplemented with 30 µM kakeimide (KKI), or on control ½ MS plates containing the solvent (DMSO) only. After 18 hours, the ultimate 10 mm root tip segments were excised, pooled, incubated for 12 h in 5 ml scintillation cocktail and the amount of radioactivity was determined by liquid scintillation counting. Four biological replicates with each 20 seedlings per replicate were assayed on identical plates containing both wild type and mutant seedlings.

Arabidopsis thaliana grafting

We used the previously reported procedure for reciprocal grafting (Turnbull, 2010). In brief, seeds were grown on 0.5xMS plates (1% agar) under long-day condition (100 µmol m^{-2} s^{-1}) at 21℃ for 5 days. Seedlings with elongated hypocotyls and similar size were cut in the hypocotyl with a sterile microsurgical blade. After the graft unions were established, the grafted plants

were examined under a stereoscopic microscope. Healthy grafted plants without adventitious roots were transferred to new plates under long-day condition. Ten days after grafting, the LR number and primary root length of the seedlings were examined.

RESULTS

GH3 are negative regulators of lateral root formation

To address the role of group II GH3s in LR formation, we analyzed the concentration dependent effects of the GH3 inhibitor, KKI that competitively inhibits IAA conjugation (Fukui *et al.*, 2022). Three-day-old seedlings were exposed for 7 days to different KKI concentrations. With increasing concentrations, both the total number of LR and the primary root length were gradually reduced. Due to the stronger root length decrease the net result was a gradual increase in LR density (Fig. **S1a-d**), and is consistent with reported effects of KKI on the root (Fukui *et al.*, 2022).

For comparison, we also explored the phenotypes of the hextuple *gh3.1/2/3/4/5/6* (*gh3hex*) mutants. Unlike the KKI treatment, the *gh3hex* mutants produced more LRs, with a slight increase in primary root length and a higher LR density than WT (Fig. **1a-d**). Of the two group II GH3s that are not mutated in *gh3hex*, GH3.17, was proposed to play a prominent role in root meristem size and root growth regulation together with GH3.5 and GH3.6 (Di Mambro *et al.*, 2019; Pierdonati *et al.*, 2019; Guo *et al.*, 2022). Consistently, *gh3.5/6/9/17*, *gh3.1/2/3/4/5/6/7 and gh3.1/2/3/4/5/6/9/17* mutants display short root phenotypes (Hayashi *et al.*, 2021; Casanova-Saez *et al.*, 2022; Guo *et al.*, 2022). Therefore, the discrepancy between the root phenotypes of the *gh3hex* mutant and KKI treatment is consistent with KKI targeting the entire group II of the GH3 family, including GH3.9 and GH3.17 (Fukui *et al.*, 2022).

The strong increase in LR density without root growth penalty highlighted *gh3hex* as an excellent tool to start unravelling the contribution of auxin conjugation in LR development.

In contrast to *gh3hex*, reported single, double and triple mutants did not show obvious LR phenotypes (Gutierrez *et al.*, 2012; Xuan *et al.*, 2015). We further explored the functional redundancy among these six GH3s by generating additional quadruple (*gh3.1/2/3/5*;

gh3.1/3/4/6; *gh3.2/4/5/6*) and quintuple (*gh3.1/2/3/4/5*; *gh3.1/2/3/5/6*; *gh3.1/2/4/5/6*; *gh3.1/3/4/5/6*; *gh3.2/3/4/5/6*) mutant combinations. Each of these mutants displayed root phenotypes that were intermediate between WT and *gh3hex* (Fig. **S2a-d**). This illustrates extensive functional redundancy between each of these GH3 in controlling LR development.

Given that amino acid conjugation of IAA precedes DAO-mediated irreversible oxidation, we also addressed the genetic interaction between *gh3hex* and *dao1-1* (Ludwig-Muller, 2011; Porco *et al.*, 2016; Hayashi *et al.*, 2021). We found that *dao1-1* only had a minor increase in LR density, and did not aggravate the *gh3hex* phenotypes in *dao1-1/gh3hex* after crossing (Fig. **1a-d**), demonstrating that *gh3hex* is epistatic to *dao1-1* in LR density control. This is consistent with the proposed model of DAO1 acting downstream of GH3 for auxin inactivation (Hayashi *et al.*, 2021). Jointly, these data support the notion that GH3.1-6 are negative regulators of LR development.

Shoot-derived auxin contributes to the increased lateral root formation in *gh3hex*

Because group II GH3s and DAO1 are implicated in auxin homeostasis, we crossed the luminescent auxin signaling reporter *DR5::LUC* into *dao1-1*, *gh3hex* and *dao1-1/gh3hex*. This reporter is not only active in morphologically detectable LR primordia, but also in pre-initiation stages of LR formation (Moreno-Risueno *et al.*, 2010; Xuan *et al.*, 2020). A spot along the primary root showing a static *DR5::LUC* expression is thus referred as a PBS. Consistent with the macroscopic root phenotypes, we found a significant increase in PBS density in *dao1-1* and *gh3hex* compared to WT (Fig. **1e-h**). Moreover, there were no significant differences between *gh3hex* and *dao1-1/gh3hex* at the level of PBS densities, corroborating their epistatic relationship. These findings suggest that at least a part of the increase in LR density results from an increase in pre-initiation events.

In analyzing the *gh3hex × DR5::LUC*, it became clear that also the auxin homeostasis of the shoot is affected, as illustrated by a very strong increase of *DR5::LUC* activity in the hypocotyl (Fig. **1e**). This suggests that GH3-mediated auxin conjugation in the shoot can attenuate the level of root branching. To address the specific contribution of shoot-expressed GH3.1-6 to LR

development we performed grafting experiments between WT and *gh3hex*. Grafting *gh3hex* shoots (= cotyledons, shoot apical meristem and leaf primordia) with WT roots resulted in enhanced LR formation (Fig. **2a,b**). Also grafting *gh3hex* roots with WT shoots resulted in significantly increased LR formation (Fig. **2a,b**). Notably, neither of the heterologous grafts performed equally well as the *gh3hex/gh3hex* graft, demonstrating that knocking out both root- and shoot-expressed GH3s contribute to the *gh3hex* LR phenotypes.

Therefore, to explore how GH3 activities in the shoot could contribute to the LR development, we applied KKI specifically to the shoot and monitored effects on root development after 3 days (Fig. **2c**). Strikingly, this localized treatment was sufficient to enhance not only *DR5::LUC* luminescence in the root, but also to increase the PBS density (Fig. **2d,e**). We assume that shoot-to-root transport of the locally applied KKI is limited, given that root growth was not significantly affected (Fig. **2d,e)**, as compared to the major effects of KKI applied directly to the root application (Fig. **S1**). This indicates that GH3 activities in the shoot inhibit LR formation. Conversely, PBS formation was abolished by shoot application of the auxin transport inhibitor NPA (*N*-1-naphthylphtalamic acid), and this could be partially reverted by co-application of KKI in WT, suggesting shoot application of NPA and KKI have opposing effects on PBS formation. We envision that the excess auxin levels under KKI treatment stimulates PIN-mediated auxin transport (Adamowski & Friml, 2015) and reduces the efficacy of NPA to inhibit PINs (Ung *et al.*, 2022). Lastly, we analyzed the effects of KKI on *d6pk0/1/3* mutants that are defective in rootward auxin transport and lack LRs (Zourelidou *et al.*, 2009; Zourelidou *et al.*, 2014; Tan *et al.*, 2020). Under control conditions this mutant was devoid of PBS (Fig. **2d,e,** Fig. **S3a**). Application of KKI to the shoot of *d6pk0/1/3* could intensify the *DR5::LUC* signal in the shoot, but could not restore PBS formation (Fig. **2d,e**), suggesting that the effect of shoot-applied KKI on LR development depends on D6PK-regulated auxin transport. In contrast, regularly spaced PBS were formed in *d6pk0/1/3* when also the roots were exposed KKI (Fig. **S3**). This indicates that the LR spacing mechanism was not affected in *d6pk0/1/3*, but that the endogenous, root auxin levels in *d6pk0/1/3* are too low to convert oscillations into PBSs. By applying KKI to the root, a critical threshold to achieve this conversion is surpassed and PBSs are formed. Jointly, these data indicate that shoot-to-root auxin transport contributes to PBS formation.

To further validate the involvement of auxin transport, we compared shoot-to-root transport of ^{3}H-IAA and ^{14}C-benzoic acid (BA) in WT and *gh3hex* in the presence or absence of KKI (Fig. **2f**). No significant differences were observed between WT and *gh3hex*, but a significant

increase in shoot-to-root transport was detected between control and KKI treated *gh3hex* (Fig. **2f**), possibly due to inhibition of the non-mutated group II GH3s (GH3.9 and GH3.17) in *gh3hex* (Fukui *et al.*, 2022). This effect on transport rates was specific to IAA, as no significant differences were observed for the diffusion control (BA) (Fig. **2f**). Jointly, these data indicate that GH3 activities in the shoot inhibit the pool of auxin that contributes to LR development.

GH3 in lateral root primordia and overlaying tissues attenuates lateral root emergence

To dissect the effects of GH3 and DAO1 in LR development in more detail, we determined the distribution of different LR developmental stages in *dao1-1*, *gh3hex* and *dao1-1/gh3hex*. The density of different LRP stages from stage I to stage VIII was very similar between all genotypes, while the number of emerged LRs was significantly higher in *gh3hex* and *dao1-1/gh3hex* than in WT and *dao1-1* (Fig. **3a**). Again, no significant differences were observed between *gh3hex* and *dao1-1/gh3hex* (Fig. **3a**). These data suggest that the density of emerged LR is enhanced due to a faster developmental progression of LRP in the *gh3hex* background. To confirm this, we used a gravistimulation-based LR synchronization assay to monitor LR developmental progression over time (Lucas *et al.*, 2008; Peret *et al.*, 2012; Voss *et al.*, 2015). Gravistimulation predictably induced a new LR in the outer bend of the reorienting root (Fig. **3b**). At each analyzed time point, we found a shift in distribution to more progressed stages of LR development in root bends of *gh3hex*, *dao1-1/gh3hex* compared to WT and *dao1-1* (Fig. **3c**), suggesting that GH3.1-6 are negative regulators of the LRP development and emergence. The lack of shifts in LRP developmental stages, despite a faster developmental progression indicates compensatory effects at the level of LR initiation.

To investigate a putative temporal differential expression of the *GH3*s in regulating the transition between LRP stages, we generated *GH3* promoter NLS-GFP/GUS reporters (*GH3pro::NLS-GFP/GUS*), and determined their expression patterns. The reporters of *GH3.1/2/5/6* were expressed within developing LRP, with *GH3.1* and *GH3.5* also being prominently expressed in LRP overlaying tissues (Fig. **3d, S4**). The reporter for *GH3.3* was only active in late stage LRPs, while the reporter for *GH3.4* was not expressed in LRPs (Fig. **3d, S4**). To assess the relevance of these expression patterns for auxin distribution during LR development, we analyzed the auxin output response marker *DR5rev::3×VENUS-N7* in *gh3hex*

mutants at different LR developmental stages. Consistent with the combinatorial *GH3* reporter expression pattern, we found stronger *DR5rev::3×VENUS-N7* expression within stage I and stage V LRPs as well as in LRP overlaying tissues when comparing *gh3hex* to WT (Fig. **3e,f**). Auxin signaling in an around a developing LRP is known to be an important determinant of the rate of its developmental progression (Swarup *et al.*, 2008; Guseman *et al.*, 2015; Stoeckle *et al.*, 2018). Our data is consistent with this model considering that GH3 expression attenuates auxin activities within developing LRP as well as in their overlaying tissues, thereby putting a brake on LRP developmental progression and emergence.

GH3s negatively regulate lateral root priming frequency

PBS derive from stabilized maxima of the oscillating *DR5::LUC* signal that can be detected close to the meristem (Moreno-Risueno *et al.*, 2010; Santos Teixeira *et al.*, 2022). Given the increase in PBS, we analyzed *DR5::LUC* dynamics in the elongation zone in the root tip of different genotypes over 22 hours. The oscillation period in *gh3hex* and *dao1-1/gh3hex* was significantly shorter than WT (Fig. **4a,b;** Video **S1**), suggesting a significant speedup of oscillations. In contrast to expectations based on the high-auxin phenotypes of *gh3hex*, the amplitude of *DR5::LUC* oscillations was significantly weaker in *gh3hex* than in WT and *dao1-1* (Fig. **4a,c;** Video **S1**). Interestingly, the *DR5::LUC* amplitude was restored in *dao1-1/gh3hex* to WT levels (Fig. **4a,c;** Video **S1**). Under the assumption that auxin accumulation is required for triggering PBS formation and that *gh3hex* and *dao1-1/gh3hex* have similar LR phenotypes, we propose that IAA levels in the oscillation zone in *gh3hex* are inefficiently translated into a *DR5::LUC* output and that this is antagonized by *dao1-1*. Similar to *gh3hex*, the *DR5::LUC* expression levels in the oscillation zone were also reduced upon KKI treatment (Fig. **S3a**), suggesting that this response is linked to impaired GH3 activity.

These data indicate that *gh3hex* has faster auxin oscillations, and that *DR5::LUC* oscillation amplitude is not strictly linked with PBS formation.

Coordination of growth and root meristem activity determines lateral root density

The oscillatory behavior of *DR5::LUC* can be explained by pulses of auxin derived from cell death in the LRC (Xuan *et al.*, 2016), and the interplay between cell division activities and auxin reflux in the meristem (van den Berg *et al.*, 2021). Therefore, both models suggest a link between oscillation frequency and meristem size.

First, we analyzed cell death rates in the LRC of *gh3hex* as estimated based on the period of disappearance of stripes of *DR5rev::3×VENUS-N7*-positive LRC cells (Xuan *et al.*, 2016). The *gh3hex* had not only more *DR5rev::3×VENUS-N7* stripes, but also showed a shorter period of *DR5rev::3×VENUS-N7* stripe disappearance (Fig. **4d-f**), which matched the increased oscillation frequency in *gh3hex* (Fig. **4a,b**). To functionally connect the increased LRC cell death rates with LRC-derived auxin in this oscillation, we used *aux1-21*, a mutant that is defective in auxin transport in the LRC, that is required for gravitropism and LR priming oscillations (Swarup *et al.*, 2005; Xuan *et al.*, 2016). The *aux1-21/gh3hex* strongly reduced the LR density of *gh3hex* (Fig. **S5a-d**), confirming the importance of LRC-derived auxin in the GH3-regulated LR density.

The increase in number of *DR5rev::3×VENUS-N7* stripes in *gh3hex* suggested an increased LRC size and associated expansion of the meristem. Indeed, meristem sizes of *dao1-1*, *gh3hex* and *dao1-1/gh3hex* were increased, with the most pronounced effects in *gh3hex* and *dao1-1/gh3hex* (Fig. **4g,h**). The transcriptional reporters of *GH3.1-6* were active in the root cap and epidermis of the root meristem (Fig. **S6b**). The reporters for *GH3.2* and *GH3.3* were active in the stem cell region and columella, and the *GH3.1* reporter was active throughout the columella, and young epidermis (Fig. **S6a,b**). With exception of *GH3.4*, all reporters displayed auxin inducibility in the root, with a prominent auxin sensitivity in the root elongation zone (Fig. **S6a**). This suggests GH3.1-6 could contribute to the auxin homeostasis in the root meristem. Consistently, *DR5rev::3×VENUS-N7* intensity was increased in the root apical meristems of *gh3hex* and *dao1-1/gh3hex* (Fig. **4i,j**). This indicates an increased auxin content, which could explain their enlarged root meristems (Mahonen *et al.*, 2014).

Therefore, the increased auxin oscillation frequency in *gh3hex* and *dao1-1/gh3hex*, could thus be explained by an increased auxin content of the root apical meristem that causes expansion of the meristem and the LRC. Previous modeling work predicts that an increase in meristem size not only results in an increase in auxin oscillation frequency, but also a decrease of priming

site density (number of priming sites relative to the number of cells the meristem produces) (van den Berg *et al.*, 2021). Still, here we observed an increase rather than a decrease in PBS density expressed as PBS per unit root length. While this increase in PBS density likely partly arises from an enhanced success rate with which auxin oscillations are translated into PBS (Santos Teixeira *et al.*, 2022), differences may also arise due to differences in cell size.

Interestingly, the increased meristem size in *gh3hex* and *dao1-1/gh3hex* was associated with a reduced elongation zone, and shorter mature cell lengths (Fig. **S7a-e**). As a consequence of this compensatory reduction of elongation, root growth rates are not greatly enhanced by the enlarged meristems, as reflected in the limited increase of root length (Fig. **1c**). Additionally, the resulting shorter cells contribute to a higher density of PBS when expressed per unit length. Therefore, the faster oscillation in combination with shorter elongated cell length and a higher oscillation result in faster production of more densely spaced PBS and LRs in *gh3hex* and *dao1-1/gh3hex*.

DISCUSSION

Ever since their discovery, GH3s have been famous for their auxin-inducibility, explaining a tight link with auxin-regulated developmental processes. In transcriptome analyses to identify new regulators of early phases of LR development, group II GH3s were always found among the top candidates (Vanneste *et al.*, 2005; De Smet *et al.*, 2007; Xuan *et al.*, 2015). Given the enzymatic activity of group II GH3s on auxin inactivation via conjugation (Staswick *et al.*, 2005; Hayashi *et al.*, 2021; Guo *et al.*, 2022), it was thus proposed that their expression at sites of organogenesis represents a negative feedback mechanism that ensures that only strong auxin signals translate into the activation of a developmental response (Vanneste & Friml, 2009). However, evaluation of this hypothesis has been hampered by extensive functional redundancy. We avoided the complexity associated with the pleiotropic root phenotype seen in higher order *gh3* mutants (Casanova-Saez *et al.*, 2021; Guo *et al.*, 2022), by analyzing GH3 function in LR development in the *gh3hex* mutant. This mutant background was selected because it had a clear increase in LR density in combination with a relatively normal root length.

The analysis of the expression patterns of *GH3.1-6*, confirmed a tight association with developing LR primordia, suggesting these GH3s attenuate auxin levels in developing LRPs and overlaying tissues. Auxin signaling intensity in the developing LRP was found to be rate-limiting for the speed of LRP development (Swarup *et al.*, 2008; Guseman *et al.*, 2015), while auxin signaling in the endodermis and cortex activates mechanisms to accommodate emergence of the developing LRP (Swarup *et al.*, 2008). Correspondingly, the increased auxin signaling levels in these tissues in *gh3hex* were matched by a faster developmental progression of LRPs.

In addition to the faster LRP development, the increased LR density was also associated with an increased density of PBS per unit of root length. We found an increased frequency for the auxin transcriptional oscillator in *gh3hex*. This increased oscillator frequency could in turn be explained by an enlarged meristem and associated increased turnover of LRC cells, jointly explaining the strong increase in LR density in *gh3hex*.

A network of auxin transporters installs a reverse fountain of auxin transport in the root meristem that ensures the re-establishment of a stable auxin gradient in the meristem after a perturbation (Motte *et al.*, 2019). Therefore, increases or reductions in root auxin content do not destroy the auxin gradient, but rather change the overall auxin concentrations across the gradient, resulting in spatial shifts in auxin responses and PLT gradients that instruct the zonation of the root meristem (Grieneisen *et al.*, 2007; Mahonen *et al.*, 2014). Consistent with the auxin-inactivating function of GH3, *gh3hex* had an enlarged root meristem that correlated with increased auxin signaling. Adhering to the principles outlined above, the auxin levels in the cells in the elongation zone are expected to also increase, thereby becoming supra-optimal or even inhibitory for cell elongation (Li *et al.*, 2021). The enlarged meristem seem to be partly compensated for by reduced cell elongation resulting only in a modest growth stimulation in *gh3hex*. In absence of further changes, an increased oscillation frequency would be expected to lower the LR density, however combined with a decrease in cell elongation and the enhanced development of oscillations into PBS and PBS into LRs we can explain the observed increase in LR density.

The expression domain of the GH3 reporters was restricted to the outer tissues of the root meristem, including the columella, LRC and epidermis, suggesting an impact on the auxin content of the shoot ward auxin flux. Disruption of this shoot ward auxin flux by introgression

of the *aux1-21* mutant greatly attenuated the effect of *gh3hex* on LR density. However, the LR density was still higher than in *aux1-21* mutant, suggesting the involvement of additional GH3-controlled auxin sources, such as the shoot. The latter is supported by grafting experiments showing that GH3 activities in the root and the shoot contribute to the *gh3hex* LR phenotype. Moreover, local application of the GH3 inhibitor KKI could increase PBS formation in an auxin transport-dependent manner. The dependence on D6PK kinases indicate the involvement of PIN-mediated auxin transport (Zourelidou *et al.*, 2014). Interestingly, the inability of *d6pk0/1/3* mutant to form discrete PBS could be restored by application of KKI to the root, suggesting that its strong LR defect is due to a lack of auxin for converting auxin oscillations into PBS.

Recently, it was proposed that DAO acts downstream, rather than parallel, of GH3-mediated auxin conjugation in the inactivation of auxin (Hayashi *et al.*, 2021). Consistently, we demonstrated epistasis of *gh3hex* over *dao1-1* in LR density, PBS density, auxin oscillations and meristem size. The limited effects of *dao1-1*, compared to *gh3hex*, on each of these phenotypes indicates that the irreversible oxidative degradation of IAA is of limited importance for auxin-dependent LR development. Contrary to expectations, in *gh3hex* the *DR5::LUC* amplitude was not increased, but reduced. This is unlikely to be an artefact of the *gh3hex* genetic background, as we observed a similar shift in *DR5::LUC* amplitude after KKI treatment. Interestingly, this reduction was restored to WT levels in the *dao1-1/gh3hex* demonstrating epistasis of *dao1-1* over *gh3hex* for *DR5::LUC* amplitude control, and thus that the change in *DR5::LUC* amplitude reflects auxin-independent effects of GH3 and DAO1. Consistent with the observed pattern of *DR5::LUC* amplitude, JA levels are increased in *gh3* mutants due to JA inactivating activities of GH3s (Gutierrez *et al.*, 2012; Casanova-Saez *et al.*, 2022), while JA levels are reduced in *dao* mutants in rice and Arabidopsis (Zhao *et al.*, 2013; Lakehal *et al.*, 2019). The resulting JA level changes could then reduce the *DR5::LUC* oscillation amplitude, in example via effects on Aux/IAA stability (Ishimaru *et al.*, 2018), but not auxin content. The high success rate in *gh3hex* of PBS formation in the absence of a high *DR5::LUC* oscillation amplitude indicates that oscillation amplitude is not a strict determinant of PBS formation.

Jointly, we clearly describe how GH3-mediated local auxin homeostasis exerts major control over all major steps in LR development. Locally expressed GH3 control the rate of LR

development and emergence via suppressing auxin levels in and around developing LRP. Earlier in LR development GH3 expression in shoot and root controls auxin levels in the root meristem, affecting the success rate with which priming oscillations become translated into stable PBS. Additionally, through auxin levels impacting meristem size and growth dynamics also oscillation frequency and hence the very first step in LR formation is modulated by GH3 Together this allows for the integration of a wide variety of signals, shoot and root localized, systemic and local, in LR development.

ACKNOWLEDGMENTS

We thank Laurence Charrier for auxin transport assays, Davy Opdenacker and Maria Njo for technical support, Joris Jourquin for providing clones, and Karin Ljung for sharing seeds. Q.W. is supported by a grant from the Chinese Scholarship Council (CSC, 201808320431).

COMPETING INTERESTS

None declared

AUTHOR CONTRIBUTIONS

TB, SV and QW designed the experiments and wrote the manuscript. QW performed most of the experiments and analyses. HDG helped with imaging, XD performed grafting experiments, MG performed and analyzed the transport assays. KT helped in interpreting experimental results in relation to LR PBS model predictions. All authors discussed the results and contributed to the finalization of the manuscript.

DATA AVAILABILITY

The data supporting the findings of this work are available within the manuscript and the Supporting Information.

REFERENCES

Adamowski M, Friml J. 2015. PIN-dependent auxin transport: action, regulation, and evolution. *Plant Cell* **27**(1): 20-32.

Ai G, Huang R, Zhang D, Li M, Li G, Li W, Ahiakpa JK, Wang Y, Hong Z, Zhang J. 2023. SlGH3.15, a member of the GH3 gene family, regulates lateral root development and gravitropism response by modulating auxin homeostasis in tomato. *Plant Sci* **330**: 111638.

Beeckman T, Engler G. 1994. An easy technique for the clearing of histochemically stained plant tissue. *Plant Mol Biol Rep* **12**: 37–42.

Benkova E, Michniewicz M, Sauer M, Teichmann T, Seifertova D, Jurgens G, Friml J. 2003. Local, efflux-dependent auxin gradients as a common module for plant organ formation. *Cell* **115**(5): 591-602.

Casanova-Saez R, Mateo-Bonmati E, Ljung K. 2021. Auxin Metabolism in Plants. *Cold Spring Harb Perspect Biol* **13**(3).

Casanova-Saez R, Mateo-Bonmati E, Simura J, Pencik A, Novak O, Staswick P, Ljung K. 2022. Inactivation of the entire Arabidopsis group II GH3s confers tolerance to salinity and water deficit. *New Phytol* **235**(1): 263-275.

Clarke JD. 2009. Cetyltrimethyl ammonium bromide (CTAB) DNA miniprep for plant DNA isolation. *Cold Spring Harb Protoc* **2009**(3): pdb prot5177.

Clough SJ, Bent AF. 1998. Floral dip: a simplified method for Agrobacterium-mediated transformation of Arabidopsis thaliana. *Plant J* **16**(6): 735-743.

De Rybel B, Vassileva V, Parizot B, Demeulenaere M, Grunewald W, Audenaert D, Van Campenhout J, Overvoorde P, Jansen L, Vanneste S, et al. 2010. A novel aux/IAA28 signaling cascade activates GATA23-dependent specification of lateral root founder cell identity. *Curr Biol* **20**(19): 1697-1706.

De Smet I, Tetsumura T, De Rybel B, Frei dit Frey N, Laplaze L, Casimiro I, Swarup R, Naudts M, Vanneste S, Audenaert D, et al. 2007. Auxin-dependent regulation of lateral root positioning in the basal meristem of Arabidopsis. *Development* **134**(4): 681-690.

Di Mambro R, Svolacchia N, Dello Ioio R, Pierdonati E, Salvi E, Pedrazzini E, Vitale A, Perilli S, Sozzani R, Benfey PN, et al. 2019. The Lateral Root Cap Acts as an Auxin Sink that Controls Meristem Size. *Curr Biol* **29**(7): 1199-1205 e1194.

Dubrovsky JG, Sauer M, Napsucialy-Mendivil S, Ivanchenko MG, Friml J, Shishkova S, Celenza J, Benkova E. 2008. Auxin acts as a local morphogenetic trigger to specify lateral root founder cells. *Proc Natl Acad Sci U S A* **105**(25): 8790-8794.

Fukui K, Arai K, Tanaka Y, Aoi Y, Kukshal V, Jez JM, Kubes MF, Napier R, Zhao Y, Kasahara H, et al. 2022. Chemical inhibition of the auxin inactivation pathway uncovers the roles of metabolic turnover in auxin homeostasis. *Proc Natl Acad Sci U S A* **119**(32): e2206869119.

Grieneisen VA, Xu J, Maree AF, Hogeweg P, Scheres B. 2007. Auxin transport is sufficient to generate a maximum and gradient guiding root growth. *Nature* **449**(7165): 1008-1013.

Guo R, Hu Y, Aoi Y, Hira H, Ge C, Dai X, Kasahara H, Zhao Y. 2022. Local conjugation of auxin by the GH3 amido synthetases is required for normal development of roots and flowers in Arabidopsis. *Biochem Biophys Res Commun* **589**: 16-22.

Guseman JM, Hellmuth A, Lanctot A, Feldman TP, Moss BL, Klavins E, Calderon Villalobos LI, Nemhauser JL. 2015. Auxin-induced degradation dynamics set the pace for lateral root development. *Development* **142**(5): 905-909.

Gutierrez L, Mongelard G, Flokova K, Pacurar DI, Novak O, Staswick P, Kowalczyk M, Pacurar M, Demailly H, Geiss G, et al. 2012. Auxin controls Arabidopsis

adventitious root initiation by regulating jasmonic acid homeostasis. *Plant Cell* **24**(6): 2515-2527.

Hayashi KI, Arai K, Aoi Y, Tanaka Y, Hira H, Guo R, Hu Y, Ge C, Zhao Y, Kasahara H, et al. 2021. The main oxidative inactivation pathway of the plant hormone auxin. *Nat Commun* **12**(1): 6752.

Heisler MG, Ohno C, Das P, Sieber P, Reddy GV, Long JA, Meyerowitz EM. 2005. Patterns of auxin transport and gene expression during primordium development revealed by live imaging of the Arabidopsis inflorescence meristem. *Curr Biol* **15**(21): 1899-1911.

Ishimaru Y, Hayashi K, Suzuki T, Fukaki H, Prusinska J, Meester C, Quareshy M, Egoshi S, Matsuura H, Takahashi K, et al. 2018. Jasmonic Acid Inhibits Auxin-Induced Lateral Rooting Independently of the CORONATINE INSENSITIVE1 Receptor. *Plant Physiol* **177**(4): 1704-1716.

Lakehal A, Dob A, Novak O, Bellini C. 2019. A DAO1-Mediated Circuit Controls Auxin and Jasmonate Crosstalk Robustness during Adventitious Root Initiation in Arabidopsis. *Int J Mol Sci* **20**(18).

Laskowski M, Ten Tusscher KH. 2017. Periodic Lateral Root Priming: What Makes It Tick? *Plant Cell* **29**(3): 432-444.

Lewis DR, Muday GK. 2009. Measurement of auxin transport in Arabidopsis thaliana. *Nat Protoc* **4**(4): 437-451.

Li L, Verstraeten I, Roosjen M, Takahashi K, Rodriguez L, Merrin J, Chen J, Shabala L, Smet W, Ren H, et al. 2021. Cell surface and intracellular auxin signalling for H(+) fluxes in root growth. *Nature* **599**(7884): 273-277.

Lucas M, Godin C, Jay-Allemand C, Laplaze L. 2008. Auxin fluxes in the root apex co-regulate gravitropism and lateral root initiation. *J Exp Bot* **59**(1): 55-66.

Ludwig-Muller J. 2011. Auxin conjugates: their role for plant development and in the evolution of land plants. *J Exp Bot* **62**(6): 1757-1773.

Mahonen AP, Ten Tusscher K, Siligato R, Smetana O, Diaz-Trivino S, Salojarvi J, Wachsman G, Prasad K, Heidstra R, Scheres B. 2014. PLETHORA gradient formation mechanism separates auxin responses. *Nature* **515**(7525): 125-129.

Malamy JE, Benfey PN. 1997. Organization and cell differentiation in lateral roots of Arabidopsis thaliana. *Development* **124**(1): 33-44.

Mellor N, Band LR, Pencik A, Novak O, Rashed A, Holman T, Wilson MH, Voss U, Bishopp A, King JR, et al. 2016. Dynamic regulation of auxin oxidase and conjugating enzymes AtDAO1 and GH3 modulates auxin homeostasis. *Proc Natl Acad Sci U S A* **113**(39): 11022-11027.

Moreno-Risueno MA, Van Norman JM, Moreno A, Zhang J, Ahnert SE, Benfey PN. 2010. Oscillating gene expression determines competence for periodic Arabidopsis root branching. *Science* **329**(5997): 1306-1311.

Motte H, Vanneste S, Beeckman T. 2019. Molecular and Environmental Regulation of Root Development. *Annu Rev Plant Biol* **70**: 465-488.

Müller K, Dobrev PI, Pencik A, Hosek P, Vondrakova Z, Filepova R, Malinska K, Brunoni F, Helusova L, Moravec T, et al. 2021. DIOXYGENASE FOR AUXIN OXIDATION 1 catalyzes the oxidation of IAA amino acid conjugates. *Plant Physiol* **187**(1): 103-115.

Nakazawa M, Yabe N, Ichikawa T, Yamamoto YY, Yoshizumi T, Hasunuma K, Matsui M. 2008. DFL1, an auxin-responsive GH3 gene homologue, negatively regulates shoot cell elongation and lateral root formation, and positively regulates the light response of hypocotyl length. *The Plant Journal* **25**(2): 213-221.

Peret B, Li G, Zhao J, Band LR, Voss U, Postaire O, Luu DT, Da Ines O, Casimiro I, Lucas M, et al. 2012. Auxin regulates aquaporin function to facilitate lateral root emergence. *Nat Cell Biol* **14**(10): 991-998.

Pierdonati E, Unterholzner SJ, Salvi E, Svolacchia N, Bertolotti G, Dello Ioio R, Sabatini S, Di Mambro R. 2019. Cytokinin-Dependent Control of GH3 Group II Family Genes in the Arabidopsis Root. *Plants (Basel)* **8**(4).

Porco S, Pencik A, Rashed A, Voss U, Casanova-Saez R, Bishopp A, Golebiowska A, Bhosale R, Swarup R, Swarup K, et al. 2016. Dioxygenase-encoding AtDAO1 gene controls IAA oxidation and homeostasis in Arabidopsis. *Proc Natl Acad Sci U S A* **113**(39): 11016-11021.

Sanchez Carranza AP, Singh A, Steinberger K, Panigrahi K, Palme K, Dovzhenko A, Dal Bosco C. 2016. Hydrolases of the ILR1-like family of Arabidopsis thaliana modulate auxin response by regulating auxin homeostasis in the endoplasmic reticulum. *Sci Rep* **6**: 24212.

Santos Teixeira J, van den Berg T, Ten Tusscher K. 2022. Complementary roles for auxin and auxin signalling revealed by reverse engineering lateral root stable prebranch site formation. *Development* **149**(22).

Schneider CA, Rasband WS, Eliceiri KW. 2012. NIH Image to ImageJ: 25 years of image analysis. *Nat Methods* **9**(7): 671-675.

Staswick PE, Serban B, Rowe M, Tiryaki I, Maldonado MT, Maldonado MC, Suza W. 2005. Characterization of an Arabidopsis enzyme family that conjugates amino acids to indole-3-acetic acid. *Plant Cell* **17**(2): 616-627.

Stoeckle D, Thellmann M, Vermeer JE. 2018. Breakout-lateral root emergence in Arabidopsis thaliana. *Curr Opin Plant Biol* **41**: 67-72.

Sugawara S, Mashiguchi K, Tanaka K, Hishiyama S, Sakai T, Hanada K, Kinoshita-Tsujimura K, Yu H, Dai X, Takebayashi Y, et al. 2015. Distinct Characteristics of Indole-3-Acetic Acid and Phenylacetic Acid, Two Common Auxins in Plants. *Plant Cell Physiol* **56**(8): 1641-1654.

Swarup K, Benkova E, Swarup R, Casimiro I, Peret B, Yang Y, Parry G, Nielsen E, De Smet I, Vanneste S, et al. 2008. The auxin influx carrier LAX3 promotes lateral root emergence. *Nat Cell Biol* **10**(8): 946-954.

Swarup R, Kargul J, Marchant A, Zadik D, Rahman A, Mills R, Yemm A, May S, Williams L, Millner P, et al. 2004. Structure-function analysis of the presumptive Arabidopsis auxin permease AUX1. *Plant Cell* **16**(11): 3069-3083.

Swarup R, Kramer EM, Perry P, Knox K, Leyser HM, Haseloff J, Beemster GT, Bhalerao R, Bennett MJ. 2005. Root gravitropism requires lateral root cap and epidermal cells for transport and response to a mobile auxin signal. *Nat Cell Biol* **7**(11): 1057-1065.

Takase T, Nakazawa M, Ishikawa A, Kawashima M, Ichikawa T, Takahashi N, Shimada H, Manabe K, Matsui M. 2004. ydk1-D, an auxin-responsive GH3 mutant that is involved in hypocotyl and root elongation. *Plant J* **37**(4): 471-483.

Takehara S, Sakuraba S, Mikami B, Yoshida H, Yoshimura H, Itoh A, Endo M, Watanabe N, Nagae T, Matsuoka M, et al. 2020. A common allosteric mechanism regulates homeostatic inactivation of auxin and gibberellin. *Nat Commun* **11**(1): 2143.

Tan S, Zhang X, Kong W, Yang XL, Molnar G, Vondrakova Z, Filepova R, Petrasek J, Friml J, Xue HW. 2020. The lipid code-dependent phosphoswitch PDK1-D6PK activates PIN-mediated auxin efflux in Arabidopsis. *Nat Plants* **6**(5): 556-569.

Turnbull CG. 2010. Grafting as a research tool. *Methods Mol Biol* **655**: 11-26.

Ung KL, Winkler M, Schulz L, Kolb M, Janacek DP, Dedic E, Stokes DL, Hammes UZ, Pedersen BP. 2022. Structures and mechanism of the plant PIN-FORMED auxin transporter. *Nature*.

van den Berg T, Yalamanchili K, de Gernier H, Santos Teixeira J, Beeckman T, Scheres B, Willemsen V, Ten Tusscher K. 2021. A reflux-and-growth mechanism explains oscillatory patterning of lateral root branching sites. *Dev Cell* **56**(15): 2176-2191 e2110.

Van Norman JM, Xuan W, Beeckman T, Benfey PN. 2013. To branch or not to branch: the role of pre-patterning in lateral root formation. *Development* **140**(21): 4301-4310.

Vanneste S, De Rybel B, Beemster GT, Ljung K, De Smet I, Van Isterdael G, Naudts M, Iida R, Gruissem W, Tasaka M, et al. 2005. Cell cycle progression in the pericycle is not sufficient for SOLITARY ROOT/IAA14-mediated lateral root initiation in Arabidopsis thaliana. *Plant Cell* **17**(11): 3035-3050.

Vanneste S, Friml J. 2009. Auxin: a trigger for change in plant development. *Cell* **136**(6): 1005-1016.

Voss U, Wilson MH, Kenobi K, Gould PD, Robertson FC, Peer WA, Lucas M, Swarup K, Casimiro I, Holman TJ, et al. 2015. The circadian clock rephases during lateral root organ initiation in Arabidopsis thaliana. *Nat Commun* **6**: 7641.

Weigel D, Glazebrook J. 2006. Transformation of agrobacterium using the freeze-thaw method. *CSH Protoc* **2006**(7).

Xuan W, Audenaert D, Parizot B, Moller BK, Njo MF, De Rybel B, De Rop G, Van Isterdael G, Mahonen AP, Vanneste S, et al. 2015. Root Cap-Derived Auxin Pre-patterns the Longitudinal Axis of the Arabidopsis Root. *Curr Biol* **25**(10): 1381-1388.

Xuan W, Band LR, Kumpf RP, Van Damme D, Parizot B, De Rop G, Opdenacker D, Moller BK, Skorzinski N, Njo MF, et al. 2016. Cyclic programmed cell death stimulates hormone signaling and root development in Arabidopsis. *Science* **351**(6271): 384-387.

Xuan W, De Gernier H, Beeckman T. 2020. The dynamic nature and regulation of the root clock. *Development* **147**(3).

Xuan W, Opdenacker D, Vanneste S, Beeckman T. 2018. Long-Term In Vivo Imaging of Luciferase-Based Reporter Gene Expression in Arabidopsis Roots. *Methods Mol Biol* **1761**: 177-190.

Zhang J, Lin JE, Harris C, Campos Mastrotti Pereira F, Wu F, Blakeslee JJ, Peer WA. 2016. DAO1 catalyzes temporal and tissue-specific oxidative inactivation of auxin in Arabidopsis thaliana. *Proc Natl Acad Sci U S A* **113**(39): 11010-11015.

Zhao Z, Zhang Y, Liu X, Zhang X, Liu S, Yu X, Ren Y, Zheng X, Zhou K, Jiang L, et al. 2013. A role for a dioxygenase in auxin metabolism and reproductive development in rice. *Dev Cell* **27**(1): 113-122.

Zheng Z, Guo Y, Novak O, Chen W, Ljung K, Noel JP, Chory J. 2016. Local auxin metabolism regulates environment-induced hypocotyl elongation. *Nat Plants* **2**: 16025.

Zourelidou M, Absmanner B, Weller B, Barbosa IC, Willige BC, Fastner A, Streit V, Port SA, Colcombet J, de la Fuente van Bentem S, et al. 2014. Auxin efflux by PIN-FORMED proteins is activated by two different protein kinases, D6 PROTEIN KINASE and PINOID. *Elife* **3**.

Zourelidou M, Muller I, Willige BC, Nill C, Jikumaru Y, Li H, Schwechheimer C. 2009. The polarly localized D6 PROTEIN KINASE is required for efficient auxin transport in Arabidopsis thaliana. *Development* **136**(4): 627-636.

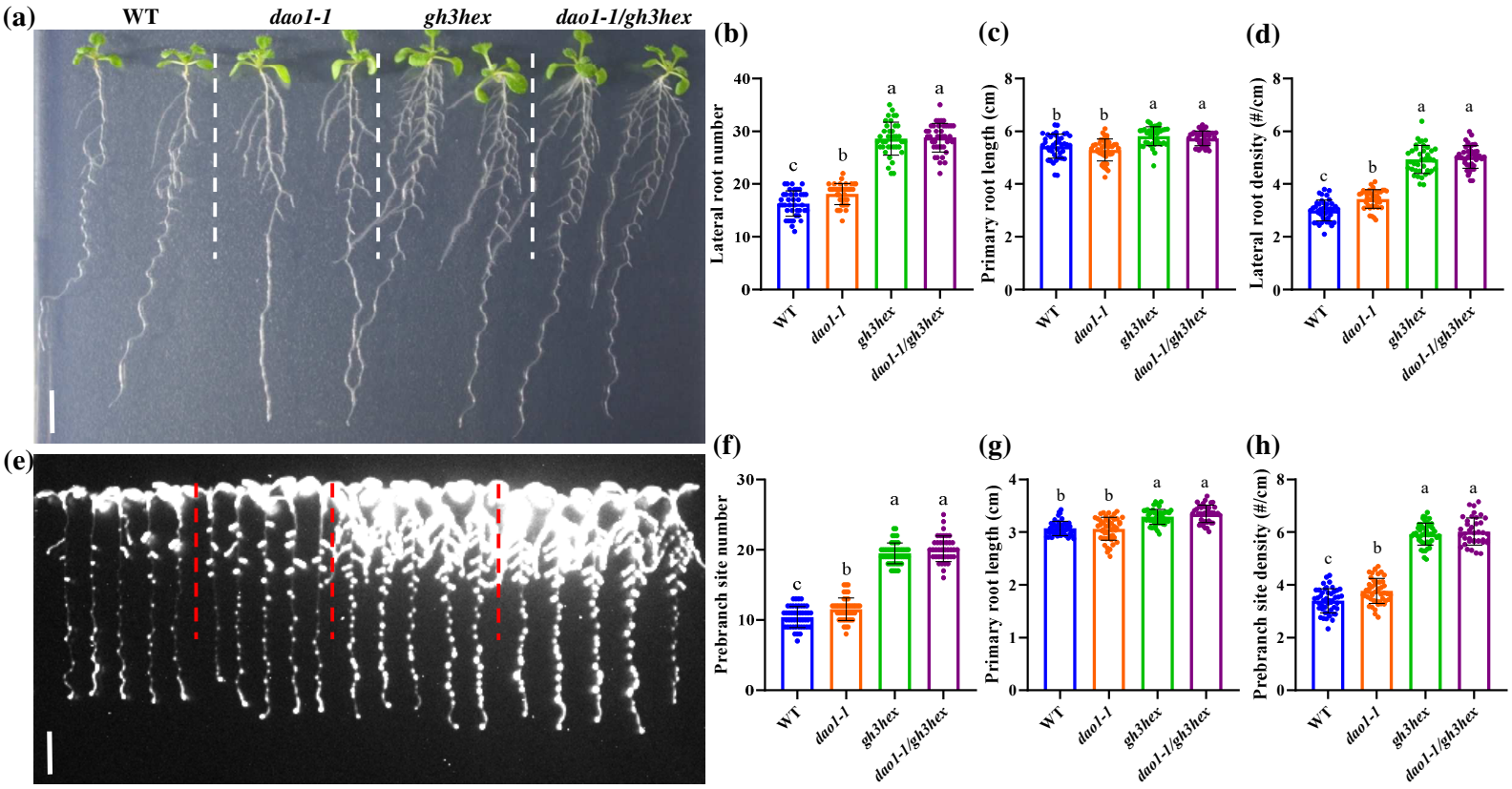

Fig. 1 GH3s are negative regulators of LR formation

(a) Root phenotype of WT (Col-0), *dao1-1*, *gh3hex* and *dao1-1/gh3hex* seedlings grown on 0.5xMS (10 days after germination; DAG). Scale = 1 cm.

(b-d) Quantification of the LR number, primary root length and LR density of WT, *dao1-1*, *gh3hex* and *dao1-1/gh3hex* in (a). Error bars represent SD (n > 30). $p<0.05$ by one-way ANOVA followed by a Tukey's multiple comparisons test. Letter code labels the significant differences.

(e) Analysis of *DR5::LUC* expression and quantification of the number of pre-branch sites, in WT , *dao1-1*, *gh3hex* and *dao1-1/gh3hex* seedlings grown on 0.5xMS (6 DAG). Scale = 1 cm.

(f-h) Quantification of the pre-branch sites number, primary root and pre-branch sites density of WT, *dao1-1*, *gh3hex* and *dao1-1/gh3hex* shown in (e). Error bars represent SD (n>20). $p<0.05$ by one-way ANOVA followed by a Tukey's multiple comparisons test. Letter code labels the significant differences between the genotypes.

.

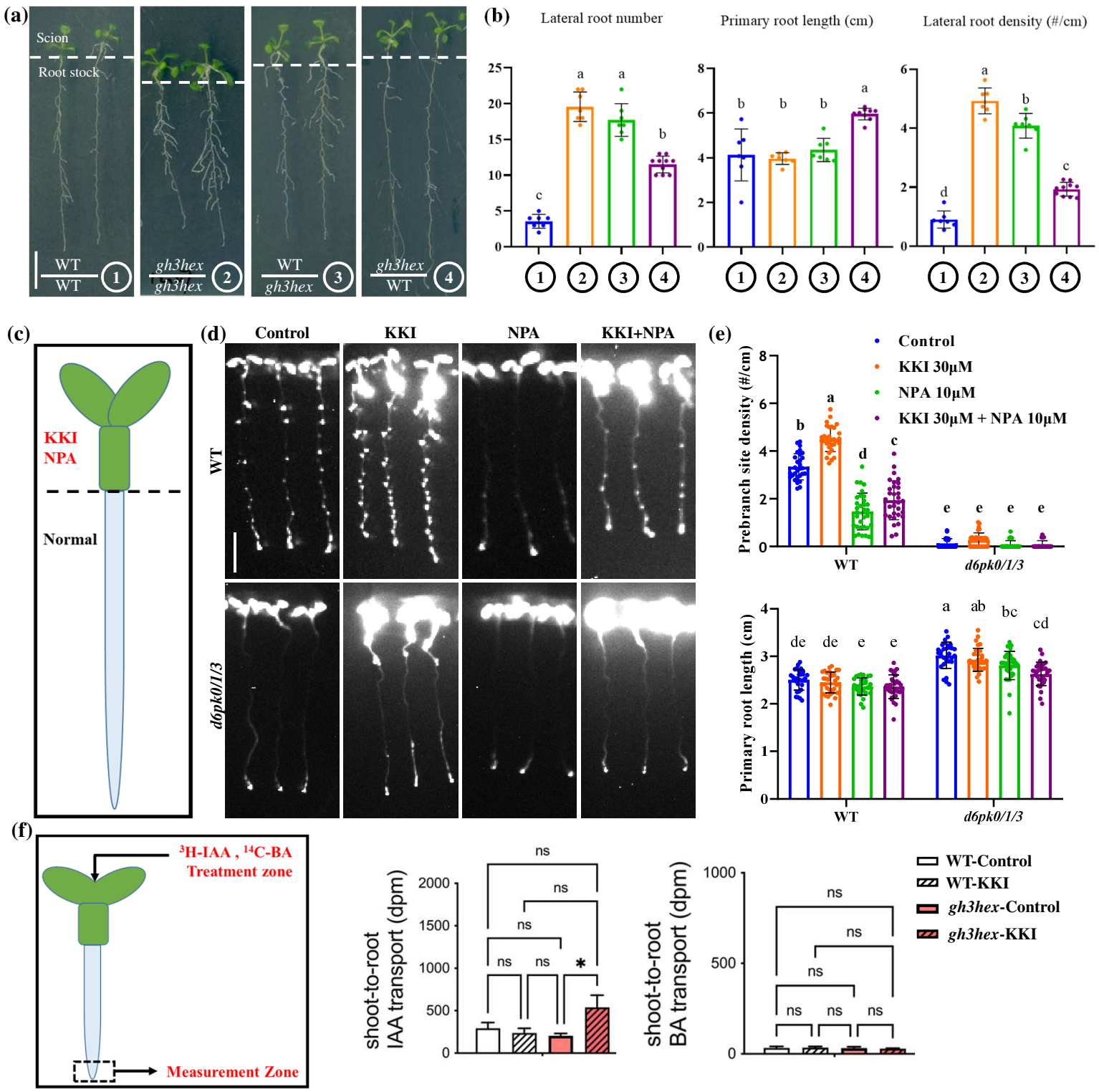

Fig. 2 GH3 activity in the shoot impacts on lateral root development

(a) The LR phenotype of different combinations grafting between WT and *gh3hex* in 13DAG seedlings. The dashed lines indicate the graft junction. Scale = 1 cm.

(b) The quantifications of LR number, PR length and LR density in seedlings depicted in (a). Error bars represent SD (n>7). $p<0.05$ by two-way ANOVA analysis followed by a Tukey's multiple comparisons test. Letter code labels the significant differences between the genotypes.

(c) Schematic representation of the shoot-specific application of KKI and NPA.

(d) Analysis of *DR5::LUC* expression of the number of PBS, in WT, *d6pk0/1/3* with KKI (30 μM) and NPA (10 μM) treatment applied to the shoot at 6 DAG for 3 days as indicated in (c). Scale = 1 cm.

(e) Quantification of the PBS density and primary root length of depicted in (d). Error bars represent SD (n>30). $p<0.05$ by two-way ANOVA analysis followed by a Tukey's multiple comparisons test. Letter code labels the significant differences between the genotypes.

(f) Schematic representation of auxin transport assay. Radiolabeled IAA (^{3}H-IAA) and BA (^{14}C-BA) were applied to the shoot, and accumulation of radioactivity in the indicated root section was determined 18h after treatment. Graphs depict the quantification of accumulation of IAA (^{3}H-IAA) and BA (^{14}C-BA) in the root tip, 18h after application to the shoot in WT and *gh3hex* treated with mock (DMSO) or KKI (30 μM). (Student's *t*-test, n= 4, $p<0.05$).

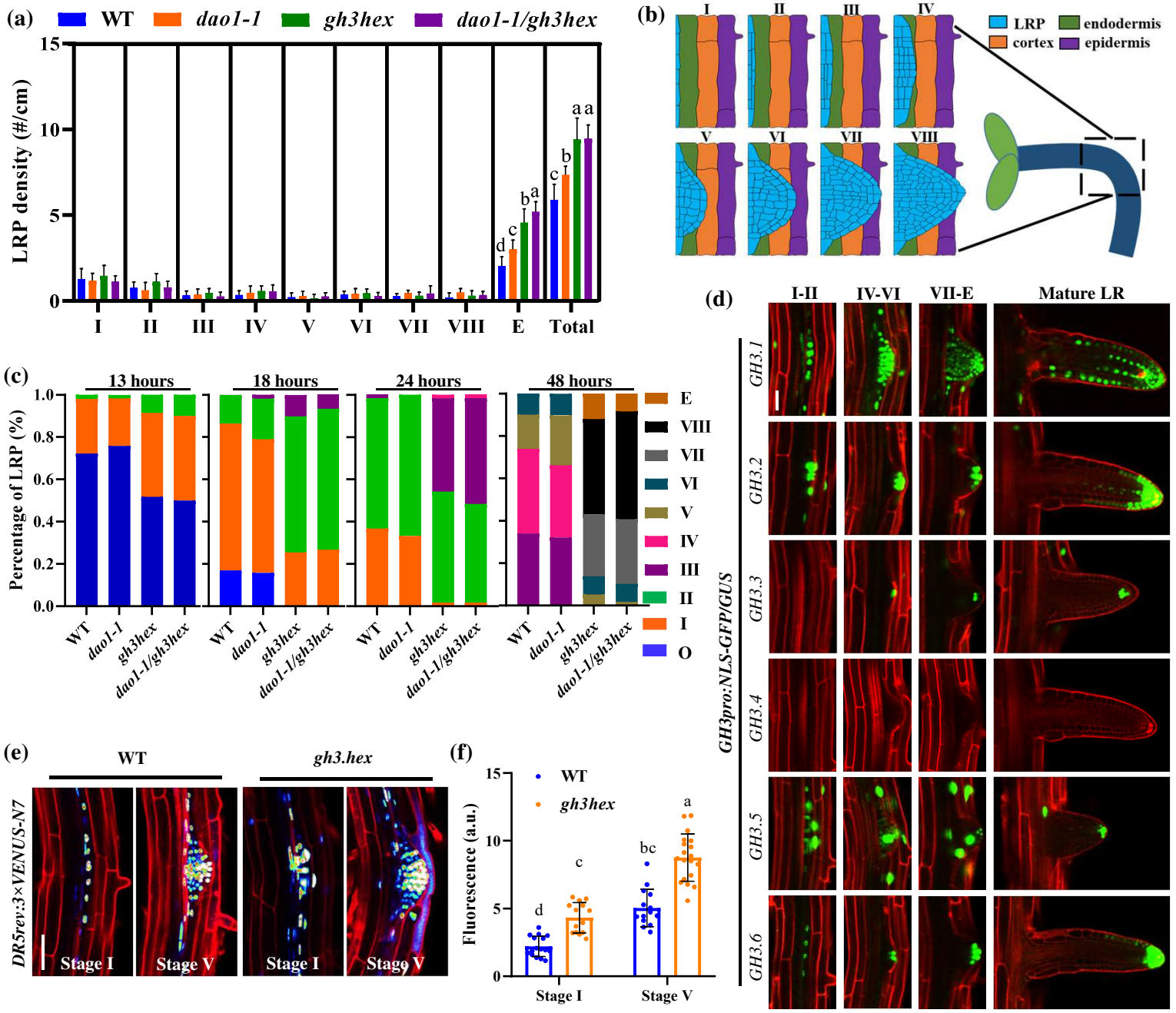

Fig. 3 GH3 expression in LRP and their overlaying tissues attenuates LR development and emergence.
(a) Quantification of LRP density in 7 DAG WT, *dao1-1*, *gh3hex* and *dao1-1/gh3hex* seedlings. Roman numerals indicate the developmental stage of LRP, and E representing emerged LR. Total is the sum of LRP and emerged LR. Error bars represent SD (n=13). $p<0.05$ by one-way ANOVA followed by a Tukey's multiple comparisons test. Letter code labels the significant differences between the genotypes per developmental stage.
(b) Schematic representation of LR synchronization via a 90° gravitropic stimulus, inducing LRP at the root bend.
(c) Distribution of developmental stages of gravistimulation-induced LRP in WT, *dao1-1*, *gh3hex* and *dao1-1/gh3hex* at 13, 18, 24 and 48 hours after gravistimulation.
(d) Expression pattern for *GH3pro::NLS-GFP/GUS* reporters for *GH3.1*, *GH3.2*, *GH3.3*, *GH3.4*, *GH3.5* and *GH3.6* in different LRP stages. Scale = 50 µm.
(e) The expression level of *DR5rev:3×VENUS-N7* in LRP in 3 DAG WT and *gh3hex* seedlings. Scale = 50 µm.
(f) Corresponding quantifications of *DR5rev:3×VENUS-N7* signal in the LRP (n>15). $p<0.05$ by one-way ANOVA followed by a Tukey's multiple comparisons test. Letter code labels the significant differences between WT and *gh3hex*.

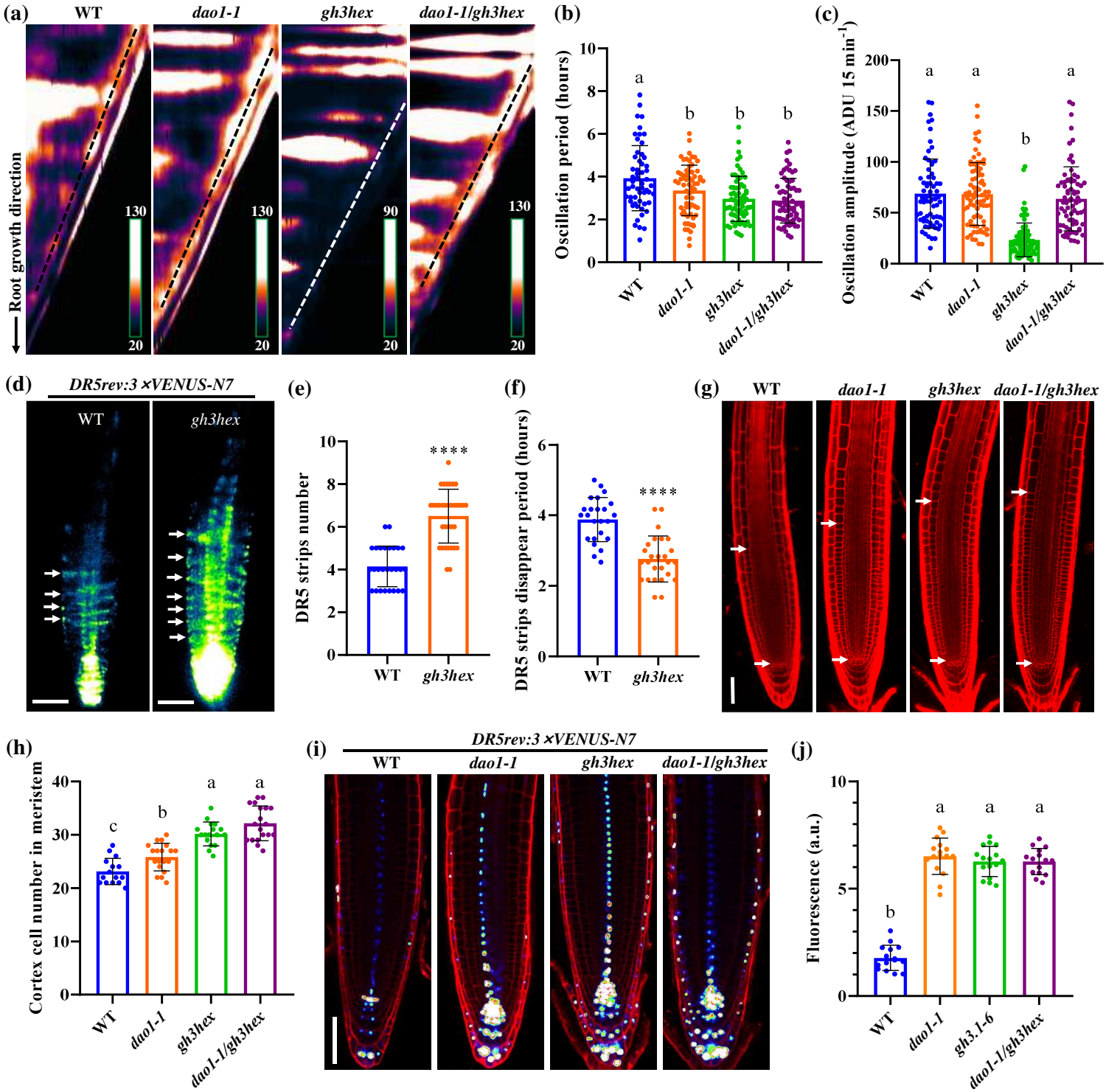

Fig. 4 Increased meristem size and LRC turnover correlates with pace of auxin oscillations in *gh3hex*.

(a) Kymograph of *DR5::LUC* intensity along the primary root of 3 DAG WT, *dao1-1*, *gh3hex* and *dao1-1/gh3hex* seedlings. DR5 luminescence intensity is color coded (see color code in the bottom left corner of the panels) and plotted following the primary root elongation (y-axis) and time (x-axis). The dashed lines indicate the position of the OZ over time.

(b-c) Boxplots showing the quantification of the oscillation frequency (b) and amplitude (c) of *DR5::LUC* in 3-day-old seedlings. Error bars represent SD (n>12). $p<0.05$ by one-way ANOVA followed by a Tukey's multiple comparisons test. Letter code labels the significant differences between the genotypes.

(d) Macroscopic view of the root meristem of *DR5rev:3×VENUS-N7* in 4 DAG WT and *gh3hex*. White arrows indicate stripes of signal derived from the LRC. Scale = 50 µm.

(e-f) Quantification of number of DR5 stripes number (e) and the period of their disappearance (f) in WT and *gh3hex* shown in (d). Error bars represent SD (n>30). $p<0.05$ by Student's *t*-test.

(g) Meristem phenotype of WT, *dao1-1*, *gh3hex* and *dao1-1/gh3hex* in 3 DAG seedlings. White arrows indicate the QC and first elongated cortex cell. Scale = 50 µm.

Legend Fig. 4 continued

(h) Quantification of meristem size of WT, *dao1-1*, *gh3hex* and *dao1-1/gh3hex* in 3 DAG seedlings, as defined by the number of non-elongated cortex cells. Error bars represent SD (n>15). p<0.05 by one-way ANOVA followed by a Tukey's multiple comparisons test. Letter code labels the significant differences between the genotypes.
(i) Confocal image of *DR5rev:3×VENUS-N7* expression in 3 DAG WT, *dao1-1*, *gh3hex* and *dao1-1/gh3hex* seedlings. Red represents PI staining; green represents VENUS-N7 signal. Scale = 50 µm.
(j) Quantification of *DR5rev:3×VENUS-N7* signal intensity in root tip (n>15). p<0.05 by one-way ANOVA analysis. Letter code labels the significant differences in 3 DAG WT, *dao1-1*, *gh3hex* and *dao1-1/gh3hex* seedlings.